

# Design of Cavity-Type and Periodic Array-Type Black Bodies with Ultra-High Emissivity

*Chong-Yang Zhang, Huan-Xin Li, Zhi-Jiao Chen, Xiao-Hai Cui, He Chen, Wei-Jun Liang, Zi-Wei Li, and Feng-Lin Yang*

**Abstract** – Black bodies provide high-precision noise temperatures for microwave radiometers, significantly improving calibration accuracy. This study employs carbonyl iron powder (CBI)-loaded epoxy as the absorbing material. Through systematic simulations and calculations, both cavity-type and periodic array-type black bodies are designed and optimized. Critical parameters, including the doping ratio of the absorbing coating, thickness, number of layers, and cone angle of the black bodies, are rigorously analyzed to achieve an ultra-high emissivity of 0.9999 within the 36- to 183-GHz frequency range.

## 1. Introduction

In microwave remote-sensing technology, high-sensitivity broadband radiometers are essential for data collection, while microwave calibration black bodies serve as indispensable tools to ensure measurement accuracy [1]. Standard black bodies provide precise noise temperature or brightness temperature signals, establishing a noise radiation reference for radiometer calibration. High-performance black bodies enhance calibration accuracy while ensuring traceability and effective value transfer, which are critical for reliable microwave remote-sensing applications.

Calibration black bodies are primarily categorized into the following two types: cavity [2, 3] and periodic array [4, 5].

- 1) Cavity-type black bodies are fabricated by coating absorbing materials on the inner walls of metallic cavities, with heaters or radiators attached to the outer walls for temperature control. Their advantages include high emissivity and uniform temperature distribution. However, their large physical

dimensions and limited effective aperture restrict their application in spaceborne or multichannel systems, rendering them more suitable for laboratory environments.

- 2) Periodic array-type black bodies typically consist of metallic bases with periodically arranged absorbers, often shaped as pyramids, wedges, or cones. Mature designs employ pyramid structures with an aspect ratio of 4, resulting in excellent absorption when combined with optimized coatings. To maintain temperature uniformity, the thickness of the absorbing coating is generally limited to 2 mm.

Both types of black bodies operate by inducing multiple reflections of incident electromagnetic waves. With each reflection, a portion of the wave energy is attenuated by the absorbing material until the reflected wave approaches zero. According to Kirchhoff's law of thermal equilibrium, emissivity = 1 – reflectivity, which explains why emissivity is indirectly measured via reflectivity.

The selection of absorbing materials is a pivotal aspect of black body design. These materials are typically composites of binders (e.g., Stycast epoxy resin) and lossy components (e.g., carbonyl iron powder [CBI], graphene, or ferrites) [6, 7]. The dielectric and magnetic properties of such composites depend on the doping ratio of the lossy material. Of note, the complex permittivity and permeability of these composites exhibit frequency-dependent behavior, resulting in variations in absorption performance across the operating band. Multilayer coatings can enhance absorption but may introduce temperature gradients and manufacturing challenges.

This study investigates cavity- and periodic array-type black bodies using CBI-loaded epoxy as the absorbing material. The effects of layer count, thickness, and doping ratio on emissivity are systematically analyzed. Two optimized black body designs are proposed as follows: one achieves an emissivity of 0.9999 within the 36- to 110-GHz band, and the other achieves an emissivity of 0.9999 within the 90- to 183-GHz band, both demonstrating exceptional performance.

## 2. Calculation of Emissivity

An ideal black body exhibits an emissivity of 1 with uniform surface temperature. In practice, emissivity is less than 1, and temperature gradients exist.

Manuscript received 5 March 2025. This work was supported by the National Key Research and Development Program of China (No. 2023YFB3905602).

Huan-Xin Li, Xiao-Hai Cui, He Chen, and Wei-Jun Liang are with Division of Electronics and Information Metrology, National Institute of Metrology, No. 18, Beisanhuan East Road, Chaoyang District, Beijing, China; e-mail: lihx@nim.ac.cn, cuixh@nim.ac.cn, chenhe@nim.ac.cn, liangwj@nim.ac.cn.

Chong-Yang Zhang, Zhi-Jiao Chen, Zi-Wei Li, and Feng-Lin Yang are with School of Electronic Engineering, Beijing University of Posts and Telecommunications, No. 10 Xitucheng Road, Haidian District, Beijing, China; e-mail: 2023110559@bupt.cn, z.chen@bupt.edu.cn, ziwei.li@bupt.edu.cn, fenglin@bupt.edu.cn.

Table 1. Fitting parameters for Havriliak-Negami model (CBI-loaded Stycast)

CBI % by vol.	$\epsilon_s$	$\epsilon_\infty$	$f_r$ (GHz)	$\alpha$	$\beta$
5	5.62	1.00	1000	0.1519	0.2433
50	13.13	10.37	85.0	$2.22e^{-14}$	1

Emissivity is calculated indirectly via reflectivity using Kirchhoff's law. This study employs geometrical optics to model the reflection paths and cumulative reflectivity of electromagnetic waves incident perpendicular to the black body aperture. Key influencing factors include:

- 1) electromagnetic properties of the absorbing material,
- 2) coating thickness and layer count, and
- 3) geometric structure of the black body.

## 2.1 Properties of Absorber

In this paper, CBI-loaded epoxy is used as a wave-absorbing material. The CBI-loaded epoxy exhibits a nonnegligible, imaginary component in its complex permeability, indicating magnetic loss characteristics.

Its frequency-dependent complex permittivity and permeability are modeled using the Havriliak-Negami and Lorentzian equations (1) and (2) [2]. Tables 1 and 2 summarize the fitting parameters for 5% and 50% CBI-loaded Stycast (an epoxy resin). The frequency-dependent real and imaginary components of  $\epsilon$  and  $\mu$  for the composite material within the 36- to 183-GHz band are illustrated in Figure 1.

$$\epsilon(f) = \epsilon_\infty + \frac{\epsilon_s - \epsilon_\infty}{\left(1 + j\left(\frac{f}{f_r}\right)^{1-\alpha}\right)^\beta} \quad (1)$$

$$\mu(f) = 1 + \frac{\mu_s - 1}{\left(1 + j\gamma\frac{f}{f_r} - \left(\frac{f}{f_r}\right)^2\right)^k} \quad (2)$$

## 2.2 Reflectance on Coatings

The reflectance at the coating surface depends on thickness, layer count, electromagnetic properties, polarization, and incidence angle, as shown in Figure 2. The reflectivity of each reflection can be calculated by (3–6), and the reflectivity of each reflection can be calculated by the geometrical optics method to further obtain the reflectivity of the black body. Accordingly, we can optimize the design of the thickness, number of layers, and concentration of the wave-absorbing coating of the black body.

Table 2. Fitting parameters for Lorentzian model (CBI-loaded Stycast)

CBI % by vol.	$\mu_s$	$f_r$ (GHz)	$k$	$\gamma$
5	8.77–4.0 j	0.859	0.8112	11.26–26.94 j
50	58.34–43.91 j	0.801	0.7487	14.57–28.41 j

$$\tilde{R}_{i,i+1} = \frac{R_{i,i+1} + \tilde{R}_{i+1,i+2}e^{-j2k_{i+1,z}d_{i+1}}}{1 + R_{i,i+1}\tilde{R}_{i+1,i+2}e^{-j2k_{i+1,z}d_{i+1}}} \quad (3)$$

$$R_{i,i+1}^{TE} = \frac{\mu_{i+1}k_{i,z} - \mu_i k_{i+1,z}}{\mu_{i+1}k_{i,z} + \mu_i k_{i+1,z}} \quad (4)$$

$$R_{i,i+1}^{TM} = \frac{\epsilon_{i+1}k_{i,z} - \epsilon_i k_{i+1,z}}{\epsilon_{i+1}k_{i,z} + \epsilon_i k_{i+1,z}} \quad (5)$$

$$k_{i,z} = \omega\sqrt{\mu_i\epsilon_i - \mu_0\epsilon_0\sin^2(\theta)} \quad (6)$$

where  $\tilde{R}_{i,i+1}$  is the total reflectance of the  $i$ -th and  $i+1$ -th coatings,  $R_{i,i+1}$  is the original reflectance on the dividing surface of the  $i$ -th and  $i+1$ -th coatings. The last layer is assumed to be a perfect electric conductor, simplifying boundary conditions ( $\tilde{R}_{i,i+1} = \pm 1$ ). From this, we can invert the formula to get the reflectivity of the surface of the outermost layer  $\tilde{R}_{0,1}$ .

## 2.3 Geometrical Optics

For both black body types, the electromagnetic wave incident perpendicular to the aperture surface is reflected on two metal walls with coatings and leaves the black body after several reflections. Therefore, in describing the physical model of this process, we can replace the electromagnetic waves incident on the black body with light rays and replace the metal reflecting surfaces covered with wave-absorbing coatings with two reflecting mirrors at a certain angle, as shown in Figure 3. In this model, the angle of the two reflecting surfaces is the top angle of the metal inner cone of the periodic array type black body or the cone angle of the cavity type black body; the top angle of the reflecting surface is located in the origin of the polar coordinate system, the center axis is located in the colinear of the coordinate axis of the polar coordinate system, and the incident electromagnetic wave is shot into the reflecting surface with the opening to the left from left to right. The angle of the two reflecting surfaces is the key parameter affecting the electromagnetic wave reflection trajectory and the number of reflections; the number of reflections and the relationship between the reflection angle and the angle of the reflecting surfaces can be expressed by (7) and (8):

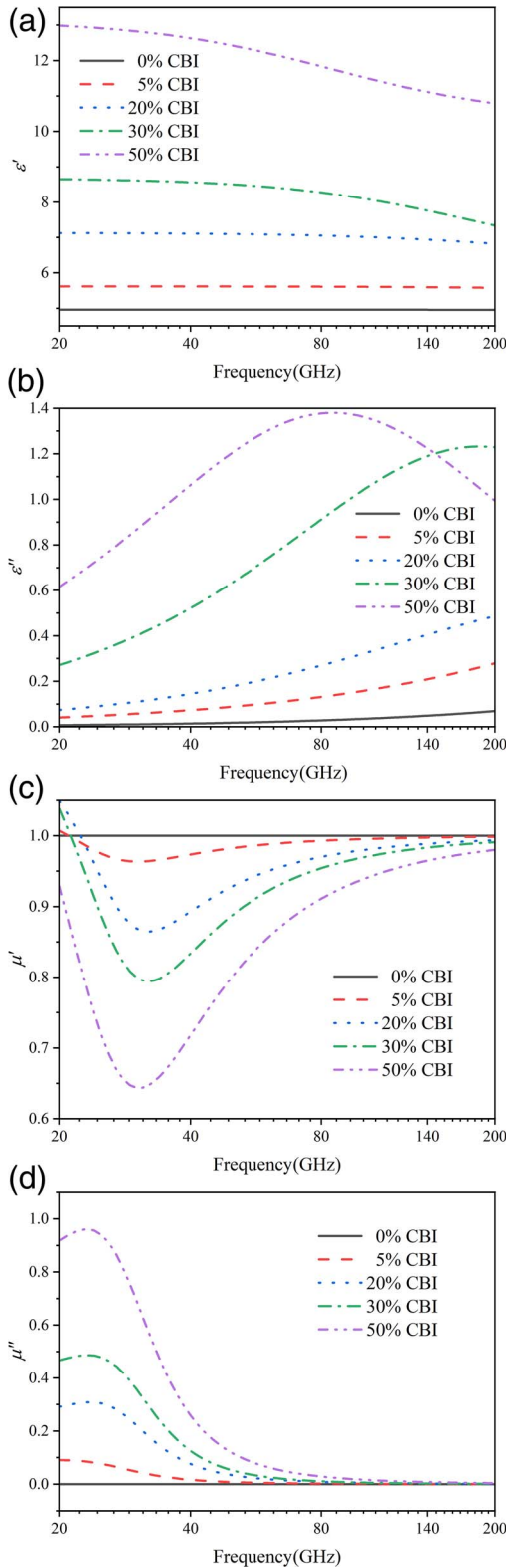


Figure 1. Frequency response of the electromagnetic properties of the mixture (CBI-loaded Styrcast) (a) The real part of the dielectric constant. (b) The imaginary part of the dielectric constant. (c) The real part of the permeability. (d) The imaginary part of the permeability.

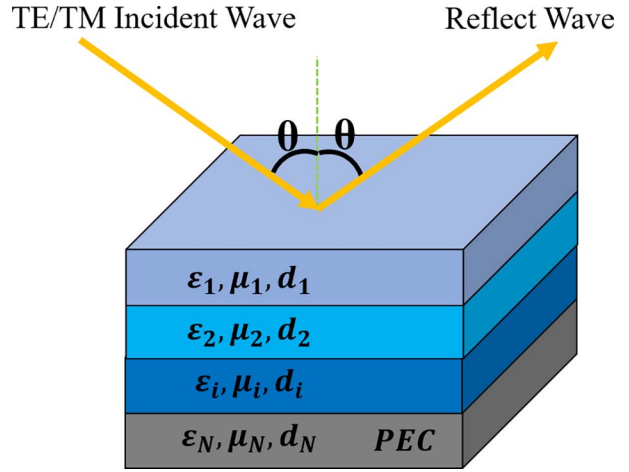


Figure 2. Schematic representation of reflectivity of multilayer wave-absorbing coatings.

$$M = \left\lceil \frac{90}{\varphi} - 0.5 \right\rceil \quad (7)$$

$$\alpha_i = (-1)^i \cdot 2i \cdot \varphi \quad (8)$$

where  $M$  is the maximum number of reflections that can occur from an electromagnetic wave incident perpendicular to the aperture plane of the black body,  $\varphi$  is the half-cone angle of the cone, and  $\alpha_i$  is the angle of the reflected wave of the  $i$ -th reflection to the polar coordinate system.

For periodic array-type black bodies, the apex region lacks metallic support, complicating wave propagation. Thus, commercial electromagnetic simulation software (e.g., CST Studio Suite) is employed for analysis, whereas cavity-type designs are evaluated using geometrical optics.

### 3. Optimization

Both periodic array- and cavity-type black body have been designed and optimized, and the detailed process is shown in the following text.

#### 3.1 Periodic Array Type

The optimization of periodic array-type black bodies involves balancing structural parameters to maximize emissivity while ensuring manufacturability. A key aspect ratio of 3.5 is selected to enhance absorption efficiency without compromising fabrication feasibility.

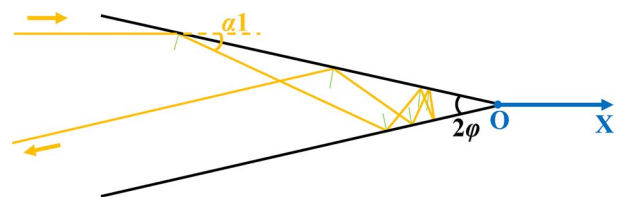


Figure 3. Physical model of geometric optics method.

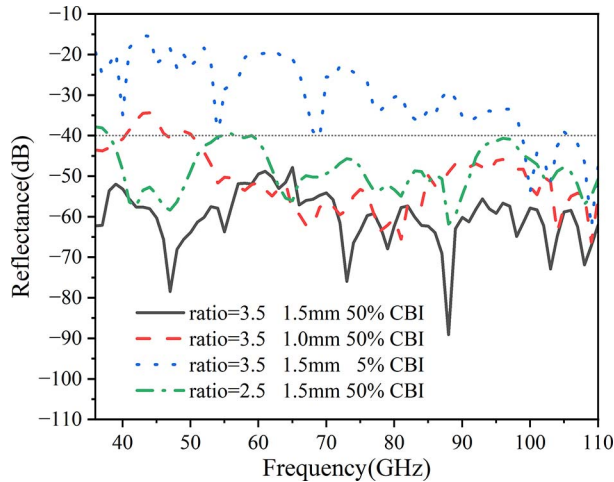


Figure 4. Comparative performance analysis of periodic array type black body (ratio is the ratio of height to width of a single element).

The absorbing coating thickness is optimized to 1.5 mm, providing sufficient attenuation of electromagnetic waves while maintaining temperature uniformity across the surface. The doping ratio of 50% CBI-loaded epoxy is identified as optimal, as it achieves effective impedance matching between air and the absorber, minimizing interfacial reflections. Excessive doping ratios are shown to degrade performance due to an increased reflection at the air-coating interface, while insufficient doping results in inadequate absorption. Figure 4 shows the emissivity of the periodic array-type black body with an aspect ratio of 3.5, a coating thickness of 1.5 mm, and a 50% concentration of CBI-loaded epoxy, as well as the emissivity of the black body when different values of these three parameters are taken.

### 3.2 Cavity Type

For cavity-type black bodies, a dual-layer coating strategy is implemented to address the trade-off between absorption depth and interfacial reflection. The first layer, with a thickness of 1.5 mm and 5% CBI doping, acts as an impedance-matching layer to facilitate the transition of electromagnetic waves from air into the absorber. The second layer, with a thickness of 9.7 mm and 50% CBI doping, serves as the primary absorbing medium. This configuration ensures broadband performance while maintaining a compact structure. The cavity's half-cone angle is set to  $10^\circ$ , and the aperture diameter is designed as 160 mm, achieving high emissivity across the 90- to 183-GHz band without excessive bulk. Figure 5 shows the performance of the cavity-type black body as the thickness of coatings is varied, where  $t_1$  denotes the thickness of 5% CBI-loaded epoxy and  $t_2$  denotes the thickness of 50% CBI-loaded epoxy.

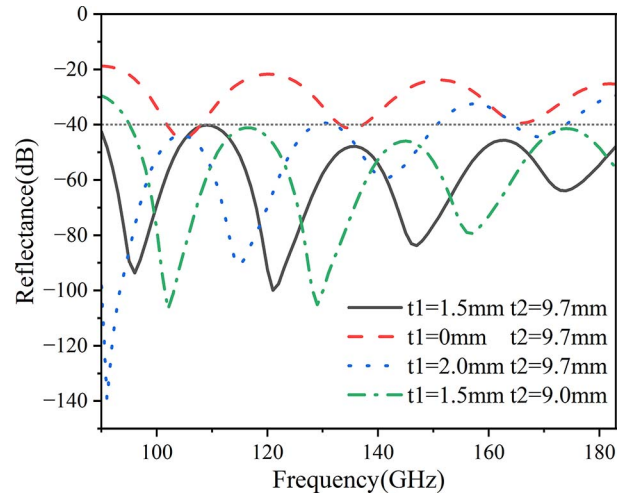


Figure 5. Comparative performance analysis of cavity-type black body ( $t_1$  denotes the thickness of 5% CBI-loaded epoxy and  $t_2$  denotes the thickness of 50% CBI-loaded epoxy).

## 4. Summary

This study presents the design and optimization of two types of black bodies—cavity- and periodic array-type—using CBI-loaded epoxy as the absorbing material. The absorption function of the black body for electromagnetic waves is realized by the wave-absorbing coating covering its surface and the conical structure of the black body. The high-emissivity performance of the black body can be achieved by choosing the appropriate wave-absorbing materials and optimizing the doping ratio of the mixture, the thickness and number of layers of the coating, and the conical structure of the blackbody. In this paper, CBI-loaded epoxy is used as wave-absorbing material in a certain proportion. For the periodic array-type black body, a periodicity of 6 mm, an aspect ratio of 3.5, and a 1.5 mm-thick 50% CBI-loaded epoxy coating are employed to achieve an emissivity of 0.9999 within the 36- to 110-GHz frequency range. The cavity-type black body features a 160-mm aperture, a  $10^\circ$  half-cone angle, and a dual-layer coating comprising a 1.5-mm 5% CBI layer and a 9.7-mm 50% CBI layer, delivering an emissivity of 0.9999 across the 90- to 183-GHz band. Both designs leverage advanced geometrical optics modeling and electromagnetic simulations to validate their performance, demonstrating their suitability for high-precision microwave radiometer calibration applications.

## 5. References

1. R. Wylde, G. Bell, A. McNamara, and A. Murk, "The Need for and Development of MM-Wave Radiometer Calibration Targets With Very Low Coherent Backscatter," 2012 Conference on Precision electromagnetic Measurements, Washington, DC, USA, July 1–6, 2012, pp. 260–261.

2. D. A. Houtz, W. Emery, D. Gu, K. Jacob, A. Murk, et al., "Electromagnetic Design and Performance of a Conical Microwave Blackbody Target for Radiometer Calibration," *IEEE Transactions on Geoscience and Remote Sensing*, **55**, 8, August 2017, pp. 4586–4596.
3. K. Jacob, A. Schröder, L. von Werra, F. Reinhard, P. Raisin, and A. Murk, "Radiometric Characterization of a Water-Based Conical Blackbody Calibration Target for Millimeter-Wave Remote Sensing," *IEEE Journal of Selected Topics in Applied Earth Observations and Remote Sensing*, **12**, 6, June 2019, pp. 1688–1696.
4. M. Jin, R. Yuan, X. Li, Y. Tao, Q. Gao, and M. Bai, "Wideband Microwave Calibration Target Design for Improved Directional Brightness Temperature Radiation," *IEEE Geoscience and Remote Sensing Letters*, **19**, May 2021, pp. 1–5.
5. T. Zou, Z. Shang, Y. Shen, Q. Wen, G. Lu, et al., "Research on Calibration Sources for a 35–40 GHz Millimeter-Wave Solar Radio Observation System," *IEEE Transactions on Antennas and Propagation*, **71**, 5, May 2023, pp. 4094–4101.
6. X. Sun, Z. Duan, and Q. Wen, "3D Lightweight Broadband Terahertz Absorber Based on Reduction Graphene Oxide," 2022 IEEE MTT-S International Microwave Workshop Series on Advanced Materials and Processes for RF and THz Applications (IMWS-AMP), Guangzhou, China, November 27–29, 2022, pp. 1–3.
7. J. Liu, Y. Tan, D. Zhang, Q. Wen, Y. Liao, et al., "Plasmonic Nanocomposite for Active Dielectric Metasurface Terahertz Absorbers," *IEEE Transactions on Terahertz Science and Technology*, **13**, 4, July 2023, pp. 381–388.